

Dynamics of Proton Transfer in Mesoscopic Clusters

Styliani Consta and Raymond Kapral
Chemical Physics Theory Group, Department of Chemistry,
University of Toronto, Toronto, Ontario, Canada M5S 1A1
(August 16, 2019)

Abstract

Proton transfer rates and mechanisms are studied in mesoscopic, liquid-state, molecular clusters. The proton transfer occurs in a proton-ion complex solvated by polar molecules comprising the cluster environment. The rates and mechanisms of the reaction are studied using both adiabatic and non-adiabatic molecular dynamics. For large molecular clusters, the proton-ion complex resides primarily on the surface of the cluster or one layer of solvent molecules inside the surface. The proton transfer occurs as the complex undergoes orientational fluctuations on the cluster surface or penetrates one solvent layer into the cluster leading to solvent configurations that favor the transfer. For smaller clusters the complex resides mostly on the surface of the cluster and proton transfer is observed only when the complex penetrates the cluster and solvent configurations that favor the proton transfer are achieved. Quantitative information on the cluster reaction rate constants is also presented.

I. INTRODUCTION

The rates and mechanisms of chemical reactions are influenced by the environments in which they occur. Clusters with linear dimensions in the mesoscopic range are especially interesting reaction environments since their properties differ from either small molecular aggregates or bulk systems. Surface forces play an essential role in the dynamics as do molecular fluctuations. Since such clusters are likely involved in the reactive processes occurring in the atmosphere, the study of their reactive dynamics has practical as well as fundamental interest.

A number of aspects of cluster reactions have been investigated recently. These investigations have examined the changes in the reactive dynamics that take place when a gas phase reaction is perturbed by clustering the reactive species with one or a few non-reactive or reactive molecules, reactive collisions where one or both of the reactive species are members of a cluster, cluster fragmentation reactions and ion-association reactions in water clusters.¹ Proton transfer barriers in small

water clusters have been computed using density functional methods² and excited state proton transfer in large water clusters has been investigated experimentally.³ The present article continues our earlier study⁴ of proton transfer in mesoscopic, polar molecular clusters. In contrast to this earlier investigation which focused on the activation free energy and its implications for the proton transfer reaction mechanism, here we consider the dynamics of the transfer process. We show that, within the mesoscopic domain, the mechanism is a function of the cluster size and describe the distinctive types of solvent dynamics that induce the proton transfer process.

The model system is essentially the same as that in our free-energy study and similar to that in other studies of proton transfer in the bulk phase.^{5,6,7,8,9} The system consists of a proton bound to a pair of A^- ions in a proton-ion complex, $(AHA)^-$. As in Refs.^{4,5,6} the distance between the two A^- ions in the complex is constrained to be 2.6\AA so that vibration of the $A - A$ bond is not considered. The proton-ion intrinsic potential was constructed to model strongly hydrogen bonded systems.¹⁰ This intrinsic potential is given by:

$$V_{int} = -\frac{1}{2}\xi_1 u^2 + \frac{1}{4}\xi_2 u^4, \quad (1)$$

where $\xi_1 = 1721.0K/\text{\AA}^2$, and $\xi_2 = 12989.0K/\text{\AA}^4$. The minima of the potential lie at $\pm 0.364\text{\AA}$ and the barrier height is about $0.2k_B T$. Here u is the proton coordinate along the ion internuclear axis measured relative to the center of the $A - A$ bond in the ion pair. In the investigation of the dynamics of the proton transfer process the proton motion is restricted to the one-dimensional coordinate u . Earlier studies of proton transfer dynamics in the bulk phase^{6,7} as well as our computations of the activation free energy for proton transfer in clusters⁴ allowed for the possibility of full three-dimensional motion of the proton. However, provided the intrinsic potential strongly confines the proton to the vicinity of the ion-pair internuclear axis, as was the case in these studies, the restriction to one-dimensional motion is an accurate representation of the dynamics. There are no fundamental difficulties in the removal of this restriction but the computation time increases.

This complex is part of a cluster of N diatomic molecules comprising the solvent. The diatomic solvent molecules are composed of two interaction sites with partial charges $z_a = \pm 0.52e$. The bond length of the diatomic molecules was fixed at 2.0\AA giving a molecular dipole moment of $\mu = 5.0D$. The interactions among solvent molecules, as well as those between the A^- ions and the solvent, arise from site-site, 6-12 Lennard-Jones (LJ) and Coulomb forces. The proton interacts with the solvent molecules via Coulomb forces. The parameters for the LJ potentials are described in.⁵

The dynamics of the transfer process



was investigated both by treating the proton degrees of freedom adiabatically and allowing for transitions among the protonic energy levels. Section II describes the

results obtained from the adiabatic simulations. This section begins with an outline of the simulation method and choice of reaction coordinate. The mechanism of the reaction that emerges from these calculations is then described, followed by a calculation of the rate constant of the reaction. Non-adiabatic dynamics is the subject of Sec. III. We first outline the surface hopping method^{9,11} which was used to carry out the non-adiabatic calculations. We then discuss the results and consider the modifications in the reaction rate and mechanism that arise as a result of non-adiabatic proton dynamics. Section IV presents a summary and discussion of the results.

II. ADIABATIC DYNAMICS

A. Simulation method

Let u be the proton coordinate and $\{\mathbf{R}\}$ the set of coordinates of all other classical particles in the system. The Schrödinger equation for the proton in the potential V_p depending on the fixed configuration $\{\mathbf{R}\}$ of the classical particles is

$$\hat{H}_p(\nabla_u, u; \{\mathbf{R}\})\Psi_n(u; \{\mathbf{R}\}) = \left[-\frac{\hbar^2}{2m_p}\nabla_u^2 + V_p(u, \{\mathbf{R}\}) \right] \Psi_n(u; \{\mathbf{R}\}) = \epsilon_n(\{\mathbf{R}\})\Psi_n(u; \{\mathbf{R}\}), \quad (3)$$

where \hat{H}_p is the total proton Hamiltonian, m_p is the mass of the proton and $2\pi\hbar$ is Planck's constant. The potential energy V_p is the sum of the intrinsic (1) and Coulomb V_c potentials, $V_p = V_{int} + V_c$. The Coulomb potential V_c is given by

$$V_c = \sum_{i,a} \frac{z_a e^2}{|\mathbf{R}_{i,a} - \mathbf{R}_{CM} - u\hat{\mathbf{R}}_{rel}|}, \quad (4)$$

here $a = 1, 2$ labels the sites of any solvent molecule i , $\mathbf{R}_{CM} = (\mathbf{R}_I + \mathbf{R}_{II})/2$ is the center of mass of the ion pair, $\hat{\mathbf{R}}_{rel} = (\mathbf{R}_I - \mathbf{R}_{II})/|\mathbf{R}_I - \mathbf{R}_{II}|$ is a unit vector directed along the ion-pair internuclear axis where \mathbf{R}_I and \mathbf{R}_{II} are the positions of the two A^- ions.

Classical particles with masses m_i evolve according to Newton's equations of motion,

$$m_i \ddot{\mathbf{R}}_i = -\nabla_{\mathbf{R}_i} V_s(\{\mathbf{R}\}) - \nabla_{\mathbf{R}_i} \langle \Psi_0(\{\mathbf{R}\}) | \hat{H}_p(\{\mathbf{R}\}) | \Psi_0(\{\mathbf{R}\}) \rangle, \quad (5)$$

where the first term is force on \mathbf{R}_i due to Coulomb and Lennard-Jones potentials that determine the solvent-solvent and solvent ion-pair interactions; the second term is the Hellmann-Feynman force that accounts for the action of the proton on the classical particles. Here $|\Psi_0(\{\mathbf{R}\})\rangle$ is the ket corresponding to the wavefunction $\Psi_0(u; \{\mathbf{R}\})$ in the u representation and $\hat{H}_p(\{\mathbf{R}\})$ is the corresponding abstract Hamiltonian.

In order to solve (3) the wave function $\Psi_n(u; \{\mathbf{R}\})$ was expanded in a linear combination of localized Gaussian functions as

$$\Psi_n(u; \{\mathbf{R}\}) = \sum_{i=1}^n c_i(\{\mathbf{R}\}) \phi_i(u) , \quad (6)$$

with

$$\phi_i(u) = \frac{1}{(2\pi\sigma_i^2)^{1/4}} e^{-(u-\mu_i)^2/(4\sigma_i^2)} , \quad (7)$$

where μ_i and σ_i denote the position and width of the Gaussian functions. The proton-ion potential restricts the proton charge density to lie within the region between the two ions and it remains localized along the internuclear axis joining the two ions. The intrinsic potential intersects the interionic axis at $\pm 0.512\text{\AA}$. Eighteen Gaussian functions were used to span the region between the A^- ions and the positions of their maxima were located at equally-spaced points μ_i between -1.0\AA and 1.0\AA . The values of the widths σ_i^2 were taken to be 0.0225\AA^2 for all basis functions. Use of the expansion given in (7) results in a standard (non-orthogonal) eigenvalue problem :

$$\mathbf{H}\mathbf{c} = \epsilon\mathbf{S}\mathbf{c} , \quad (8)$$

where \mathbf{H} is the Hamiltonian matrix with elements

$$H_{ij} = \int \phi_i(u) H_p(\nabla_u, u; \{\mathbf{R}\}) \phi_j(u) du , \quad (9)$$

and \mathbf{S} is the overlap matrix with elements

$$S_{ij} = \int \phi_i(u) \phi_j(u) du . \quad (10)$$

The coefficients c_i satisfy the normalization condition

$$\sum_{i,j}^n c_i S_{ij} c_j = 1 . \quad (11)$$

The adiabatic dynamics calculation was performed as follows : The Schrödinger equation (8) was solved for the ground state wave function and energy for a given configuration of classical particles. Note that the distance between the ions A^- is kept fixed so the time-dependent contribution to the potential arises from the positions of the solvent molecules in the cluster. Then, using the ground state wave function, the Hellman-Feynman forces given in (5) were computed and the classical equations of motion (5) were integrated to yield a new classical configuration. The Verlet algorithm¹² was used with time step of $5 \times 10^{-15} s$ to integrate the classical equations. The constraints used to fix the intramolecular bond lengths were treated using the SHAKE algorithm.¹³ The constant temperature simulations were carried out using Nosé dynamics.¹⁴

B. Rate constant

One of the first steps in the study the rate of a reaction is the choice of a reaction coordinate. For adiabatic dynamics a natural choice for the proton transfer reaction coordinate is the expectation value of the position of the proton, $\bar{z}_p(\{\mathbf{R}\}) = \langle \Psi_0(\{\mathbf{R}\}) | u | \Psi_0(\{\mathbf{R}\}) \rangle$. As we shall see, this reaction coordinate does provide a useful description of the proton transfer reaction dynamics. However, since it depends on the expansion coefficients of the ground state wave function which are known only numerically, it is convenient to seek an alternative reaction coordinate whose form is known analytically. Following earlier proton transfer studies⁵ we use as a reaction coordinate the solvent polarization^{15,16} given by,

$$\Delta E(\{\mathbf{R}\}) = \sum_{i,a} z_a e \left(\frac{1}{|\mathbf{R}_i^a - \mathbf{s}|} - \frac{1}{|\mathbf{R}_i^a - \mathbf{s}'|} \right). \quad (12)$$

Here \mathbf{s} and \mathbf{s}' are two points along the ion-pair axis in the reactant and product regions. We shall show that both the expectation value of the proton position and the solvent polarization provide equivalent descriptions of the reaction dynamics and either is a good reaction coordinate.

Proton transfer in clusters is an activated process⁴ and if the free energy barrier is high enough a direct estimate of the reaction rate will require a long molecular dynamics trajectory. In this circumstance it is necessary estimate the reaction rate coefficient directly from the reactive-flux correlation function.¹⁷ Using the polarization reaction coordinate, the (time-dependent) rate constant is given by

$$k(t) = \frac{\langle \Delta \dot{E}(0) \delta(\Delta E(0) - \Delta E^\ddagger) \theta[\Delta E(t) - \Delta E^\ddagger] \rangle}{\langle \theta[\Delta E(t) - \Delta E^\ddagger] \rangle} = k^{TST} \kappa(t). \quad (13)$$

where the angular brackets represent a canonical ensemble average, $\theta(\Delta E(t))$ is the Heaviside function and ΔE^\ddagger is the value of the reaction coordinate at the barrier top ($\Delta E^\ddagger = 0$ for our symmetrical case). The rate constant is equal to the product of the transition state theory (TST) estimate of the rate constant and the transmission coefficient $\kappa(t)$. Using the Constrained-Reaction-Coordinate Dynamics (CRCDD) ensemble¹⁸ the transmission coefficient is given by,

$$\kappa(t) = \frac{\langle D^{-1/2} \Delta \dot{E} \theta[\Delta E(t)] \rangle_c}{\langle D^{-1/2} \Delta \dot{E} \theta(\Delta \dot{E}) \rangle_c}, \quad (14)$$

where $\langle \dots \rangle_c$ is an ensemble average in the CRCDD ensemble where the configurational distribution is taken from the $\Delta E = 0$ constrained dynamics but the velocity distribution is that for the system with no $\Delta E = 0$ constraint. The correction factor D that removes the bias generated by sampling initial configuration conditions from the constrained trajectories. For the polarization reaction coordinate D is simply given by,

$$D = \frac{1}{2m} \sum_i \left[\sum_a \nabla_{i,a} \Delta E \right]^2, \quad (15)$$

where $m = m_i$ is the common mass of a solvent atom, i runs over the number of molecules and $a = 1, 2$. The TST result may be computed from the expression:¹⁸

$$k^{TST} = (2\pi\beta)^{-1/2} \frac{\langle \delta(\Delta E - \Delta E^\ddagger) \rangle}{\langle D^{-1/2} \rangle_c \langle \theta(\Delta E - \Delta E^\ddagger) \rangle}. \quad (16)$$

C. Simulation results

Calculations were performed for clusters of $N = 20$ and $N = 67$ solvent molecules at temperatures of $200K$ and $260K$, respectively. Under these conditions the clusters were in the liquid state. Evaporation did not occur on the time scale of the simulations, typically several nanoseconds.

The fact that either the average proton position or the solvent polarization constitute acceptable reaction coordinates is demonstrated in Fig. 1 which shows that the time variations of both coordinates track the hops of the proton between the reactant and product configurations. Consequently we shall use both coordinates to provide insight into the reaction mechanism and for the computation of the rate constant.

1. proton transfer mechanism

The proton transfer mechanism consists of the description of the solvent dynamics in the course of the reaction (2). In our study of the proton transfer activation free energy we discussed the differences in the cluster structure when the proton was constrained to lie in the transition state or reactant (or product) regions.⁴ We may now describe the dynamical changes in the solvent that accompany the transfer of the proton in the complex.

We begin by confirming the picture of the cluster structure that emerged from the free energy study where a Feynman path integral representation of the proton degrees of freedom was used and the centroid¹⁹ of the proton “polymer” was taken to be the reaction coordinate.⁴ We consider the probability density, $\rho_\pm(z, r)$, for finding a positive or negative site on a solvent molecule at a point (z, r) in a cylindrical coordinate system centered on the $A - A$ ion pair of the proton-ion complex with z directed along the $A - A$ axis and r the radial coordinate in this cylindrical frame. The probability density is averaged over the angle variable. Rather than constructing this quantity by constraining the reaction coordinate to lie in the transition state or reactant (product) regions as was the case in Ref.,⁴ here we simply construct this quantity from a long unconstrained adiabatic molecular dynamics run and collect statistics for the probability density histogram only when the reaction coordinate

is found in the reactant or product configurations. The results of this calculation are shown in Fig. 2 for a cluster with 20 solvent molecules and in Fig. 3 for a 67-molecule cluster. The insets in these figures show schematically the configuration of the proton-ion complex for the parts of the trajectory used to collect the statistics.

The structural ordering in the cluster is evident in these figures. The cluster solvent molecules tend to strongly solvate the part of the proton-ion complex with the more exposed negative charge; i.e., the end of the complex which is less strongly bonded to the H^+ ion. This suggests that the complex tends to “float” on the surface of the cluster. When the H^+ ion is strongly bound to one A^- ion, this $A-H$ dipole has a smaller dipole moment than that of a solvent molecule. Consequently, the solvent-solvent interactions are stronger than the interactions between a solvent molecule and this part of the proton-ion complex. These energetic arguments suggest that it may be favorable for this end of the proton-ion complex to reside on the surface of the cluster, a fact borne out by our simulation results. Of course, both entropic as well as energetic factors come into play in determining the structure of mixed clusters²¹ but here energetic factors seem to play a dominant role.

There is also clear evidence of orientational order as can be seen from a comparison of the densities for the positive and negative sites. The same general picture applies for both the 20 and 67-molecules clusters. However, the 67-molecules cluster is large enough to support two solvent shells around the proton-ion complex and the presence of this second solvent shell has some important consequences for the dynamics which we shall describe below. The picture that emerges from these results is consistent with that from the earlier free energy studies: the position of the proton in the proton-ion complex has a strong influence on the structure of the cluster.

Insight into the reaction mechanism can be obtained by examining the correlation between the time variation of the reaction coordinate and the solvent-complex dynamics. Let \mathbf{d}_i be the vector from the center of mass of the complex to that of the i^{th} solvent molecule, $\mathbf{d}_i = \frac{1}{2}(\mathbf{R}_{i,1} + \mathbf{R}_{i,2}) - \mathbf{R}_{CM} = \mathbf{R}_i^{CM} - \mathbf{R}_{CM}$, and \mathbf{d} the vector from the center of mass of the complex to the center of mass of the solvent molecules in the cluster

$$\mathbf{d} = N^{-1} \sum_{i=1}^N \mathbf{R}_i^{CM} - \mathbf{R}_{CM} = N^{-1} \sum_{i=1}^N \mathbf{d}_i . \quad (17)$$

Two quantities were used to gain insight into the nature of the solvent-complex dynamics: $d = |\mathbf{d}|$ and $n^* = n_+ - n_- = \sum_{i=1}^N (\theta(\mathbf{d} \cdot \mathbf{d}_i) - \theta(-\mathbf{d} \cdot \mathbf{d}_i)) = -N + 2 \sum_{i=1}^N \theta(\mathbf{d} \cdot \mathbf{d}_i)$. Here $\theta(x)$ is the Heaviside function and n_+ and n_- are the number of solvent molecules with $\mathbf{d} \cdot \mathbf{d}_i > 0$ and $\mathbf{d} \cdot \mathbf{d}_i < 0$, respectively. One expects small values of d when the complex is near the center of the cluster and large values when the complex is on the surface. Similarly, n^* varies between $n^* = 0$ when the complex is symmetrically solvated in the center of the cluster and $n^* = N$ when it lies on the surface of a symmetrical cluster. It is possible to construct cluster configurations where the conditions are violated. Nevertheless, these quantities provide useful

indicators for solvent-complex dynamics and we have confirmed all aspects of our interpretations by direct visualization of the cluster dynamics.

The results are shown in Figs. 4 and 5. In the case of a 20-molecule cluster one sees that the complex resides for long portions of time on the surface of the cluster (average distance $d \sim 6$) and long portions of time in the interior of the cluster (average distance $d \sim 2$). If the complex is on the surface of the cluster then transitions rarely occur; however, if the complex makes an excursion into the interior (see the first large dip in n^* and d in Fig. 4) then this excursion correlates with a proton transfer.²⁰ If the complex resides in the interior of the cluster, as is the case for times between 2.0 and 4.0 ns in the figure, then proton transfer events are frequent.

The picture is somewhat different for the 67-molecule cluster. The proton-ion complex rarely penetrates deeply into the cluster. Some of the proton transfer events correlate with excursions of the complex into the cluster, but only one solvent layer deep and never far from the surface. However, even when the complex “floats” on the surface of the cluster there are frequent proton transfer events. Such events were not observed in the 20-molecule cluster case (although they may occur with lower frequency on longer time scales). The mechanism of these transfer events becomes clear from an examination of Fig. 6 which shows cluster configurations including the complex during one proton transfer event. Initially, the proton (black) is strongly bound to the “white” ion in the complex. The complex resides on the surface of the cluster with its “gray” end solvated in the cluster and its white end extending out of the cluster. In the course of time a fluctuation occurs that causes the complex to assume a configuration parallel to the surface so that there is a more nearly equal solvation of the two ends of the complex. This is a favorable configuration for proton transfer and transfer takes place around frame (d) of this figure. Once the proton transfer is complete, then the favorable complex configuration is for the now strongly hydrogen bonded gray end to protrude from the cluster and the weakly bound white end to lie within the cluster.

Thus, the mechanism of the proton transfer depends on the size of the cluster. For smaller clusters fluctuations lead to penetration of the complex into the interior of the cluster where proton transfer is likely. For larger clusters transitions occur primarily by orientational motion of the complex on the surface of the cluster or when the complex makes shallow penetrations into the cluster. Deep penetrations of the complex into the cluster are rare. For the smaller 20-molecule cluster, presumably the orientational motion of the complex is restricted on the surface due to the larger surface forces. These features are borne out by an examination of the radial probability densities of the distance d , $R_c(d)$ shown in Fig. 7 (a) for a 20-molecule cluster and in (b) for a 67-molecule cluster. For the 20-molecule cluster there are two peaks, one corresponding to molecules in the interior of the cluster and the other for molecules on the surface. The results for the 67-molecule cluster show a broad single peak, with indications of some structure, corresponding to molecules on the surface and just within the cluster.

2. rate constant

We now turn to a quantitative treatment of the reaction rate and compute the value of the rate constant. As described above, this calculation can be divided into two parts: the calculation of the TST estimate of the rate constant and the transmission coefficient. The product of these quantities yields the full rate constant.

We begin with the computation of the TST rate constant using (16). The numerator of this expression is proportional to the probability density of finding the reaction coordinate at the barrier top ($\Delta E = 0$) which in turn is related to the exponential of the activation free energy. The free energy may be computed using the CRCDD ensemble or estimated directly from a long unconstrained molecular dynamics trajectory if transitions are frequent. Figure 8 shows the free energy along the reaction coordinate determined in this way for a 67-molecule cluster along with the quadratic approximations to the results determined from fits around the potential minima. Note the parabolic nature of the free energy in the vicinities of the minima; in fact, the quadratic approximation is quite accurate over the entire range except at the barrier top where one expects the quadratic extrapolation to overestimate the barrier height. The direct simulation is also most subject to error at the barrier top where the probability density is smallest and here one expects the direct simulation to underestimate the barrier height. If one estimates the free energy barrier from the average of these two results one finds $W(0) = 4.47\text{kT}$ for the 67-molecule cluster. Using (16) one finds $k^{TST} = 0.04\text{ps}^{-1} = 1/25.0\text{ps}$. The corresponding results for the 20-molecule cluster are: $W(0) = 7.75\text{kT}$ and $k^{TST} = 0.025\text{ps}^{-1} = 1/40.0\text{ps}$.

The TST rate constant may also be estimated from the analytical formula

$$k^{TST} = \frac{\omega_0}{2\pi} e^{-W(0)/kT} , \quad (18)$$

where ω_0 is the frequency corresponding to the free energy minima. For comparison we may compute k^{TST} using this formula along with the free energy determined from the proton position reaction coordinate instead of the solvent polarization coordinate. The results of this computation are: $k^{TST} = 0.036\text{ps}^{-1} = 1/28.0\text{ps}$ for the 67-molecule cluster and $k^{TST} = 0.014\text{ps}^{-1} = 1/69.4\text{ps}$ for the 20-molecule cluster. The results for the 67-molecule cluster are in quite good agreement and the somewhat poorer results for the 20-molecule cluster arise from an inaccurate knowledge of the barrier height.

The transmission coefficient was computed using (14). The following method was used to calculate the averages in the CRCDD ensemble: Statistically independent classical configurations were selected every 10 ps from a long (1 ns in the case of 20 solvent molecule cluster and 1.24 ns in the case of 67 solvent molecule cluster) constant temperature Nosé molecular dynamics trajectory where the polarization reaction coordinate was constrained to lie at the transition state ($\Delta E = 0$). Initial velocities were assigned according to the generalization of Boltzmann sampling for rigid diatomic molecules.²² For this ensemble of initial conditions, the constraint on

the polarization coordinate was released and the trajectories were evolved forward in time using microcanonical molecular dynamics. This ensemble of trajectories could then be used to generate the averages needed to compute (14).

Figures 9 (a) and (b), respectively, show the transmission coefficients as a function of time for the 67 and 20-molecule clusters. From these graphs the transmission coefficients may be determined from the plateau values and one finds $\kappa = 0.4$ and $\kappa = 0.5$ for the 67 and 20-molecule clusters, respectively. The results in these figures show a rapid decay on a time scale which is less than a picosecond followed by a somewhat longer decay, of the order of a few picoseconds, to a plateau value. The time scale for the establishment of a plateau in $\kappa(t)$ is longer in the cluster environment than in the bulk⁵ for a similar but not identical intrinsic potential. This again signals different dynamics in the cluster compared to the bulk.

The full rate constants determined from the product of k^{TST} and κ are $k = 1/62.5\text{ps}$ and $k = 1/80.0\text{ps}$ for the 67 and 20-molecule clusters, respectively. Finally, we may estimate the rate constant directly by simply monitoring the number of proton transfers in a long unconstrained adiabatic molecular dynamics trajectory. This procedure yields $k = 1/88\text{ps}$ for a 67-molecule cluster where the unconstrained trajectory had 77 proton transfer events. For a 20-molecule cluster where the trajectory had 29 transfer events the estimated rate is $k = 1/190\text{ps}$. Once again the 67-molecule results are in good agreement. However, for the smaller 20-molecule cluster, since the free energy barrier is higher and the quadratic approximation is valid over a smaller range it is more difficult to estimate the barrier height. In addition, proton transfer is a more rare event so that the direct estimate of the rate is also subject to uncertainties. For these reasons the rate estimates are more variable for the 20-molecule cluster.

III. NON-ADIABATIC DYNAMICS

A. Simulation method

The effect of non-adiabatic dynamics on the computation of the rate of the reaction was taken into account by using Tully’s surface-hopping, stochastic model^{11,9} which accounts for the possibility of quantum transitions in the dynamics of mixed quantum-classical systems.

In this method a group of “classical trajectories” is considered. Each classical trajectory is evolved according to an equation of motion similar to (5) but with Ψ_0 replaced by Ψ_n , any of the adiabatic functions. The Hamiltonian (3) characterizes the quantum system. The wave function $\Phi(u, \mathbf{R}, t)$ that describes the quantum mechanical state at time t , is expanded as a linear combination of the adiabatic states for the instantaneous “classical configuration”,

$$\Phi(u, \{\mathbf{R}\}, t) = \sum_n C_n(t) \Psi_n(u; \{\mathbf{R}\}), \quad (19)$$

where C_n are complex-valued expansion coefficients. Substitution of the above equation into Schrödinger equation yields the following equation for the evolution of the expansion coefficients:

$$i\hbar\dot{\tilde{C}}_k = \tilde{C}_k(V_{kk} - V_{00}) - i\hbar \sum_j \tilde{C}_j \dot{\mathbf{R}} \cdot \mathbf{d}_{kj}. \quad (20)$$

where

$$\tilde{C}_j = C_j \exp(i \int_0^t dt' V_{00}/\hbar). \quad (21)$$

Furthermore, using abstract notation

$$V_{kj}(\{\mathbf{R}\}) = \langle \Psi_i(\{\mathbf{R}\}) | \hat{H}_p(\{\mathbf{R}\}) | \Psi_j(\{\mathbf{R}\}) \rangle, \quad (22)$$

and the non-adiabatic coupling vector $\mathbf{d}_{kj}(\{\mathbf{R}\})$ is defined as

$$\mathbf{d}_{kj}(\{\mathbf{R}\}) = \langle \Psi_k(\{\mathbf{R}\}) | \nabla_{\{\mathbf{R}\}} | \Psi_j(\{\mathbf{R}\}) \rangle. \quad (23)$$

Equations (20) are integrated simultaneously with the classical equations of motion. Let denote by Δ the classical time step and δ the quantum time step. At the end of each classical time step it is determined if a quantum transition has taken place. According to the “fewest switches” algorithm the probability of switching from the current state k to all other states j during the time interval between t and $t + \Delta$ is

$$g_{kj} = \frac{b_{jk}(t + \Delta)\Delta}{a_{kk}(t + \Delta)}, \quad (24)$$

where $a_{kj} = C_k C_j^*$ and $b_{jk} = -2\text{Re}(a_{jk}^* \dot{\mathbf{R}} \cdot \mathbf{d}_{kj})$. If g_{kj} is negative, it is set equal to zero.

The simulation method is described in Ref.⁹ Specifically, our simulations were carried out as follows: Three quantum adiabatic states were used to describe the state of the proton. Initial conditions for a group of “classical trajectories” were determined. Statistically independent classical configurations were selected every 10 ps from a long canonical run where the polarization reaction coordinate was constrained at zero. Initial velocities were assigned according to the generalization of Boltzmann statistics for rigid diatomic molecules.²² Initially the total population was taken to be in the ground state, so $\tilde{C}_0 = 1.0$. For each of the “classical trajectories”, initially two adiabatic steps were carried out to obtain the non-adiabatic coupling vector. Using the wave function Ψ_k the Hellmann-Feynman forces were computed. The classical equations (5) with Ψ_0 replaced by Ψ_k were integrated using the RAT-TLE algorithm²³ with a time step of $\Delta = 1 \times 10^{-2}$ ps. When the expectation value of proton position entered the transition region, $-0.42 < \langle \Psi_k(t) | u | \Psi_k(t) \rangle < 0.42$, starting from the previous time step, the integration step of the classical equations of motion was changed to $\Delta = 10^{-3}$ ps and integration was continued for 150 time

steps. Equations (20) were integrated using the Runge-Kutta method with time step $\delta = 10^{-5}$ ps. At the end of each classical time step the switching probability was computed using (24) to determine if a switch occurred. If a switch occurred conservation of the energy was satisfied by redistribution of the kinetic energy. Between transitions the coefficients $C_k(t)$ evolve coherently. When $\langle \Psi_k(t-\Delta) | u | \Psi_k(t-\Delta) \rangle < 0.59\text{\AA} < \langle \Psi_k(t) | u | \Psi_k(t) \rangle$ or $\langle \Psi_k(t) | u | \Psi_k(t) \rangle < -0.59\text{\AA} < \langle \Psi_k(t-\Delta) | u | \Psi_k(t-\Delta) \rangle$, so that the proton density enters the reactant or product regions, the coefficient for the current state was set equal to one, and all the other coefficients were set equal to zero.

B. simulation results

We may now examine the effects of transitions among the protonic states on the proton transfer dynamics. Figure 10 shows a sample non-adiabatic trajectory for a 67-molecule cluster. The lower panel in the figure is the proton position reaction coordinate computed using $\bar{z}_p^n = \langle \Psi_n | u | \Psi_n \rangle$, while the upper panel shows in which of the three states the proton lies. We note that the polarization coordinate is also a good reaction coordinate in the non-adiabatic case since it tracks the proton density changes. A number of features of these non-adiabatic trajectories are noteworthy.

As expected, there is a strong correlation between transitions among the protonic energy states and the proton transfer events. The probability of a transition is large when the separation between the adiabatic energy levels is small and the separation is smallest in the transition region. Proton transfer does, of course, occur in the absence of transitions to the excited protonic states in accord with the predictions of adiabatic dynamics but there are substantial modifications to the simple adiabatic model because the separation between the ground and first adiabatic states is comparable to kT in the transition region. When the system is in an excited protonic state there is an increased probability of a proton transfer event. The proton density is more diffuse in the excited states than in the ground state. Also, when the system is in an excited protonic state and the reaction coordinate lies in the transition state region, the proton probability density is higher at extended spatial points where the proton ground state density is low. As a result, the proton density affects the solvent through Hellman-Feynman forces in ways that favour the transition state configurations. Consequently, when the proton is in the excited states re-crossings of the transition state region are more frequent than when it is in the ground state. This effect can be seen in the figure where the number of proton transfer events, and attempted proton transfer events, is larger when the system is in the excited states than when it is in the ground state.

From these trajectories the picture of the proton transfer process is quite different from that for adiabatic dynamics since many proton transfer events are accompanied by transitions to an excited protonic state. If the system makes a transition to an excited state it does not remain there long and quickly returns to the ground

state so that the majority of time is spent in the ground state configuration. From the simulation results we estimated that the proton remains in excited states for only about 22 per cent of the total time. Thus, while in the course of passage from the reactant to the product regions the proton may make transitions into and out of an excited state, most of the dynamics is controlled by the ground state wave function.

For non-adiabatic dynamics, the rate constant of the reaction was computed directly by dividing the time of the run by the number of proton transfers between product and reactant states. The simulation employed five trajectories (each 0.5 ns in duration) that followed microcanonical dynamics. The average temperature of the system was 260K. The rate constant was estimated to be $k = 0.017ps^{-1}$ (1/59.0 ps) which is in good agreement with the adiabatic result. The fact that the rate in the non-adiabatic case is very close to that computed using adiabatic dynamics most likely arises from a cancellation of effects: when transitions to an excited protonic state occur and there is an increased probability of proton transfer, there is also an increased number of re-crossings in the transition region which lead to a small transmission coefficient and reduce the rate.

IV. CONCLUSION

Proton transfer rates and mechanisms differ significantly in the cluster and bulk environments. As in the bulk, solvation forces play an important role in determining the character of the cluster reaction but these solvation forces have a distinctive character in the cluster. In the model investigated in this paper, the $A - H$ end of the proton-ion complex, for instance in the configuration $(A - H \cdots A)^-$, experiences interactions with the solvent dipolar molecules that are weaker than the solvent-solvent interactions. The $\cdots A^-$ end of the complex with the more exposed negative charge experiences strong charge-dipole interactions with the solvent molecules. These specific forces are responsible for the tendency of the complex to reside on the surface of the cluster when the proton is in the reactant or product configurations and for the fact that the complex tends to be oriented normal to the surface with the $\cdots A^-$ in the cluster.

There are strong fluctuations in these mesoscopic, liquid-state clusters. If the cluster is small enough, as in the 20-molecule clusters studied here, the complex resides predominantly on the surface of the cluster and reaction occurs only when it penetrates into the cluster. For larger clusters, e.g. the 67-molecule cluster, the complex again resides predominantly on the surface or one layer of solvent molecules inside the surface but now transfer is observed on the cluster surface as well.

One may consider extensions of these ideas to other situations. Whenever there is strong charge separation in the course of reaction one might envisage scenarios like the one described above. However, the solvation forces could favor solvation of the complex in the interior of the cluster. This, in turn, would possibly give rise to

a transfer mechanism similar to that in the bulk phase. The interplay between the specific solvation forces, cluster size and the nature of the reactive species merits further investigation.

The model for proton transfer considered here, that of a strongly hydrogen bonded system with negligible intrinsic barrier, favors the applicability of adiabatic dynamics. Nevertheless, we saw that although adiabatic dynamics does provide an estimate of the rate constant, transitions to excited states do occur and they have implications for the mechanism. Thus, it is interesting to investigate weakly hydrogen bonded systems where non-adiabatic effects are even larger and could lead to a different picture of the proton transfer process.

ACKNOWLEDGMENTS

This work was supported in part by a grant from the Natural Sciences and Engineering Research Council of Canada and a Killam Research Fellowship (R.K.).

REFERENCES

- [1] See, for example, A.W. Castleman, Jr. and R.G. Keesee, *Science* **241**, 36 (1988); R.G. Keesee and A.W. Castleman, Jr., *J. Phys. Chem. Ref. Data*, **15**, 1011 (1986); R. Naamen, *Adv. Chem. Phys.* **70**, 181 (1988); H.-P. Kaukonen, U. Landman and C.L. Cleveland, *J. Chem. Phys.* **97**, 4997 (1991) and references therein; D. Laria and R. Fernández-Prini, *Chem. Phys. Lett.* **205**, 260 (1993); D. Laria and R. Fernández-Prini, *J. Chem. Phys.* (1995), to be published; *Reaction Dynamics in Clusters and Condensed Phases*, eds. J. Jortner, et al. (Kluwer Academic Publishers, Dordrecht, 1994).
- [2] D. Wei and D. Salahub, *J. Chem. Phys.* **101**, 7633 (1994).
- [3] R. Knochenmuss, G. Holtom and D. Ray, *Chem. Phys. Lett.*, **215**, 188 (1993).
- [4] S. Consta and R. Kapral, *J. Chem. Phys.*, **101**, 10908 (1994).
- [5] D. Laria, G. Ciccotti, M. Ferrario, R. Kapral, *J. Chem. Phys.*, **97**, 378 (1992).
- [6] D. Laria, G. Ciccotti, M. Ferrario, R. Kapral, *Chem. Phys.* **180**, 181 (1994).
- [7] D. Li and G. Voth, *J. Phys. Chem.* **95**, 10425 (1991).
- [8] D. Borgis and J.T. Hynes, *J. Chem. Phys.* **94**, 3619 (1991); D. Borgis, G. Tarjus, H. Azzouz, *J. Phys. Chem.* **96**, 3188 (1992); D. Borgis, G. Tarjus, H. Azzouz, *J. Phys. Chem.* **97**, 1390 (1993); H. Azzouz and D. Borgis, *J. Phys. Chem.* **98**, 7361 (1993).
- [9] S. Hammes-Schiffer and J.C. Tully, *J. Chem. Phys.*, **101**, 4657 (1994).
- [10] See, for instance, M.D. Joesten and L.J. Schaad, *Hydrogen Bonding*, (Marcel Dekker, Inc., NY, 1974).
- [11] J. C. Tully, *J. Chem. Phys.*, **93**, 1061 (1990); J. C. Tully, *Int. J. Quantum Chem. Quantum Chem. Symp.*, **25**, 299 (1991).
- [12] L. Verlet, *Phys.Rev.*, **159**, 98 (1967).
- [13] J.P. Ryckaert, G. Ciccotti, and H.J.C. Berendsen, *J. Comput. Phys.*, **23**, 327 (1977).
- [14] S. Nosé, *Mol. Phys.*, **52**, 255 (1984); W.G. Hoover, *Phys. Rev. A*, **31**, 1695 (1985).
- [15] R.A. Marcus and N. Sutin, *Biochim. Biophys. Acta*, **811** 265 (1985).
- [16] A. Warshel *J. Am. Chem. Soc.*, **86**, 2218 (1982).
- [17] T. Yamamoto, *J. Chem. Phys.* **33**, 281 (1960); D. Chandler, *J. Chem. Phys.* **68**, 2959 (1978).
- [18] E. Carter, G. Ciccotti, J.T. Hynes, R. Kapral, *Chem. Phys. Lett.*, **156**, 472 (1989).
- [19] M. Gillan, *J. Phys. C* **20**, 3621 (1987); G. A. Voth, D. Chandler and W. H. Miller, *J. Chem. Phys.* **91**, 7749 (1989).
- [20] The quantity n^* shows more reliably the location of the complex in the cluster than the distance d . For instance, in Fig. 4 in the vicinity of 2.6 ns the values of d suggest that the complex is inside the cluster while the values of n^* suggest that the complex is on the surface. Apart from such infrequent discrepancies, in our simulations the conclusions drawn from both indicators are generally the same.

- [21] A.S. Clarke, R. Kapral, B. Moore, G. Patey and X.-G. Wu, Phys. Rev. Lett. **70**, 3283 (1993); A.S. Clarke, R. Kapral and G. Patey, J. Chem. Phys. **101**, 2432 (1994).
- [22] G. Ciccotti and J. P. Ryckaert, Comp.Phys.Rep. **4**, 345 (1986).
- [23] H. C. Andersen, J. Comput. Phys. **52**, 24 (1983).

FIGURES

FIG. 1. Comparison of the proton position, \bar{z}_p , and solvent polarization, ΔE (in units of $10^{-21}C/\text{\AA}$), reaction coordinates. These reaction coordinates are plotted as a function of time for a $N = 20$ molecule cluster.

FIG. 2. Probability density of (a) the positive and (b) the negative solvent-ion sites in a cylindrical coordinate system centered on the proton-ion complex for a 20 molecule cluster. The z axis is along the $A - A$ interionic axis and r is the distance to a solvent-ion site from the interionic axis of the $A - A$ ion pair. The probability density was constructed by collecting configurations every 1.25 ps while the proton charge density is found between $\pm 0.7\text{\AA}$ and $\pm 1.0\text{\AA}$.

FIG. 3. Solvent ion probability densities. Same as Fig. 2 but for a 67-molecule cluster. The probability density was constructed by collecting configurations every 2.5 ps while the proton charge density is found between $\pm 0.7\text{\AA}$ and $\pm 1.0\text{\AA}$.

FIG. 4. Trajectory of the proton position, \bar{z}_p (top panel), the distance d between the center of mass of the cluster and the center of mass of the ion-pair (middle panel) and $n^* = n_+ - n_-$ (bottom panel) as a function of time for a 20-molecule cluster.

FIG. 5. Same as Fig. 4 but for a 67-molecule cluster.

FIG. 6. Cluster configurations during a proton transfer event for a 67-molecule cluster. The configurations are separated by 2.5 ps. Time increases from panel (a) to panel (f).

FIG. 7. Radial probability density $R_c(d) = 4\pi\rho(d)d^2$ versus d the distance between the center of mass of the ion pair and the center of mass of the solvent for (a) a 20-molecule cluster and (b) a 67-molecule cluster. The configurations used to construct these densities were collected every 1.25 ps for the 20-molecule cluster and every 2.5 ps for the 67-molecule cluster in the course of 4 ns unconstrained trajectories.

FIG. 8. Free energy along the polarization coordinate for a 67-solvent molecule cluster. The open circles are the results from an unconstrained trajectory of 4 ns duration. The line is computed from the least-squares quadratic approximation to the numerical results at the free energy minima.

FIG. 9. Transmission coefficient as a function of time for (a) a 67-solvent molecule cluster and (b) a 20-solvent molecule cluster.

FIG. 10. Non-adiabatic dynamics trajectory. The upper panel shows the protonic states and the lower panel gives the proton position reaction coordinate as a function of time. The error bars represent \pm one standard deviation.

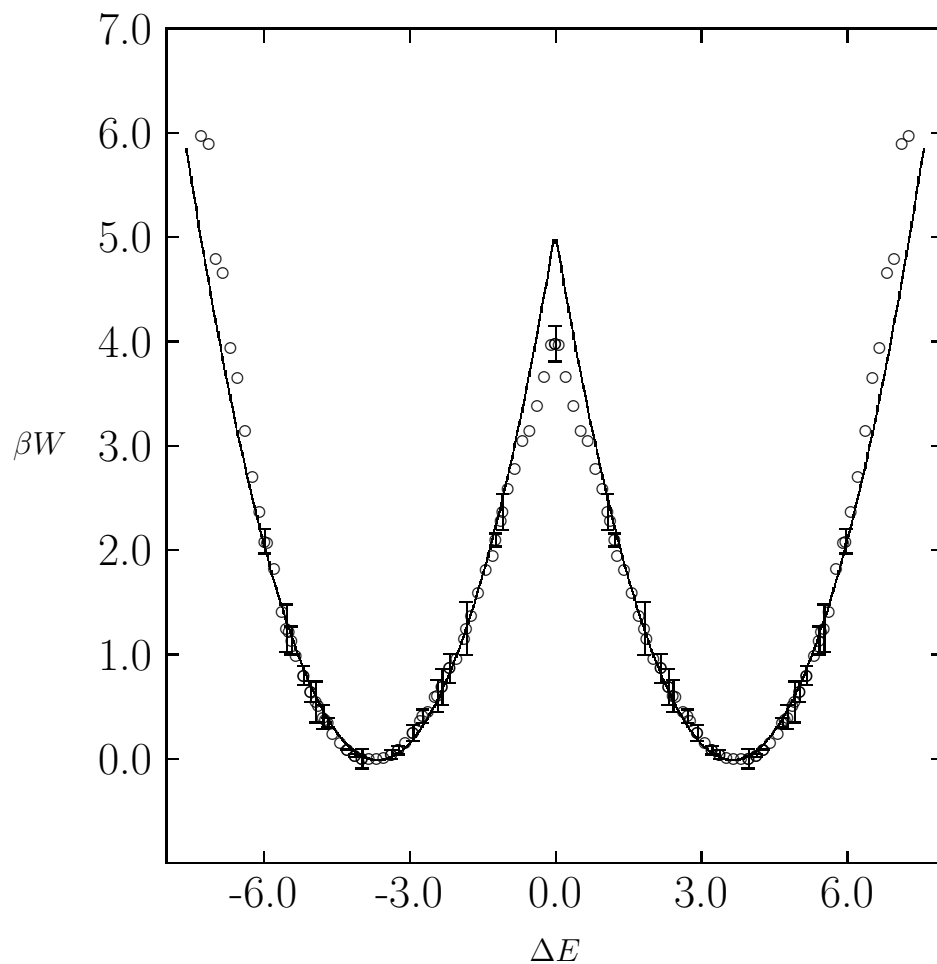


FIG. 11. Free energy along the polarization coordinate for a 67-solvent molecule cluster. The open circles are the results from an unconstrained trajectory of 4 ns duration. The line is computed from the least-squares quadratic approximation to the numerical results at the free energy minima.

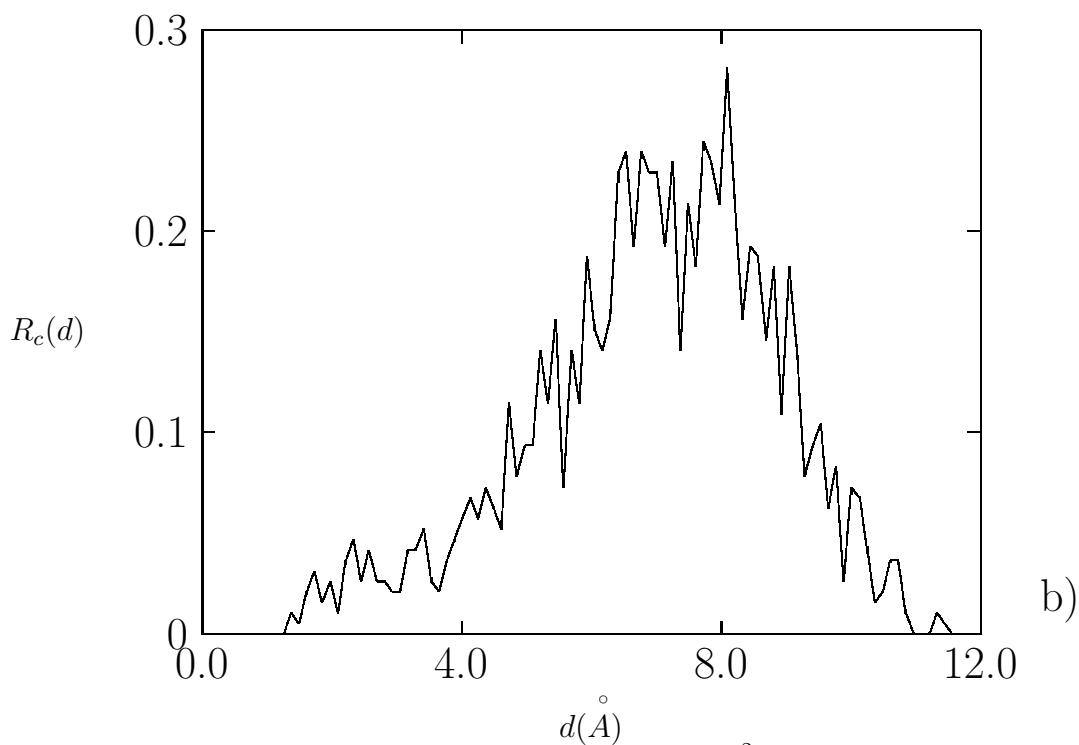
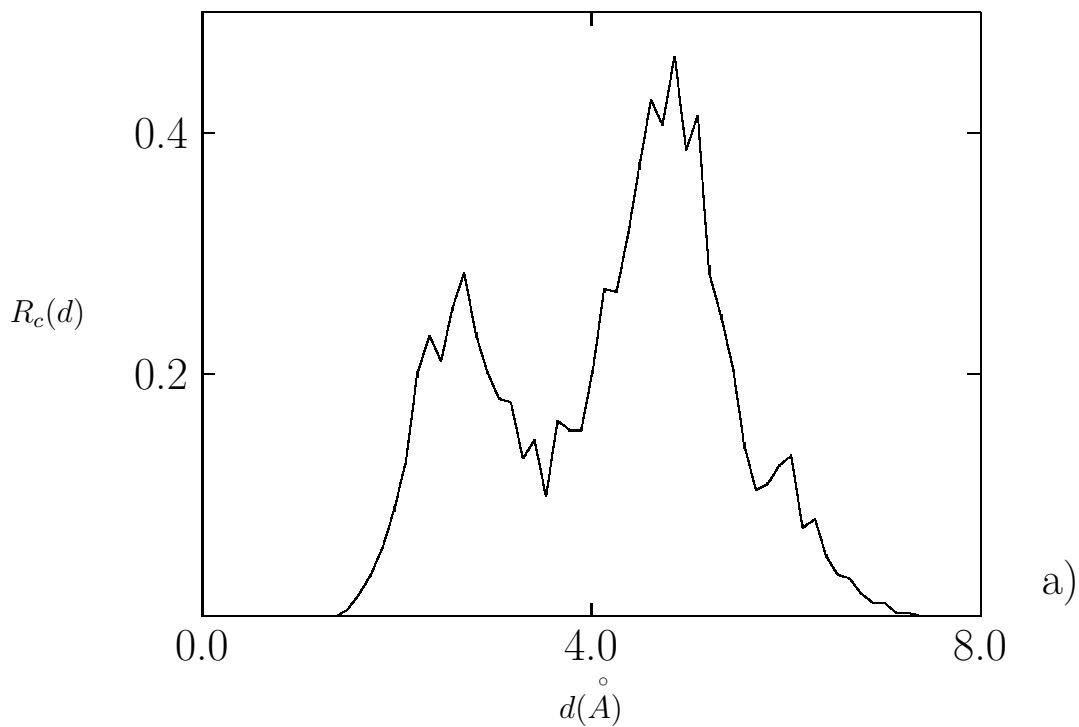


FIG. 12. Radial probability density $R_c(d) = 4\pi\rho(d)d^2$ versus d the distance between the center of mass of the ion pair and the center of mass of the solvent for (a) a 20-molecule cluster and (b) a 67-molecule cluster. The configurations used to construct these densities were collected every 1.25 ps for the 20-molecule cluster and every 2.5 ps for the 67-molecule cluster in the course of 4 ns unconstrained trajectories.

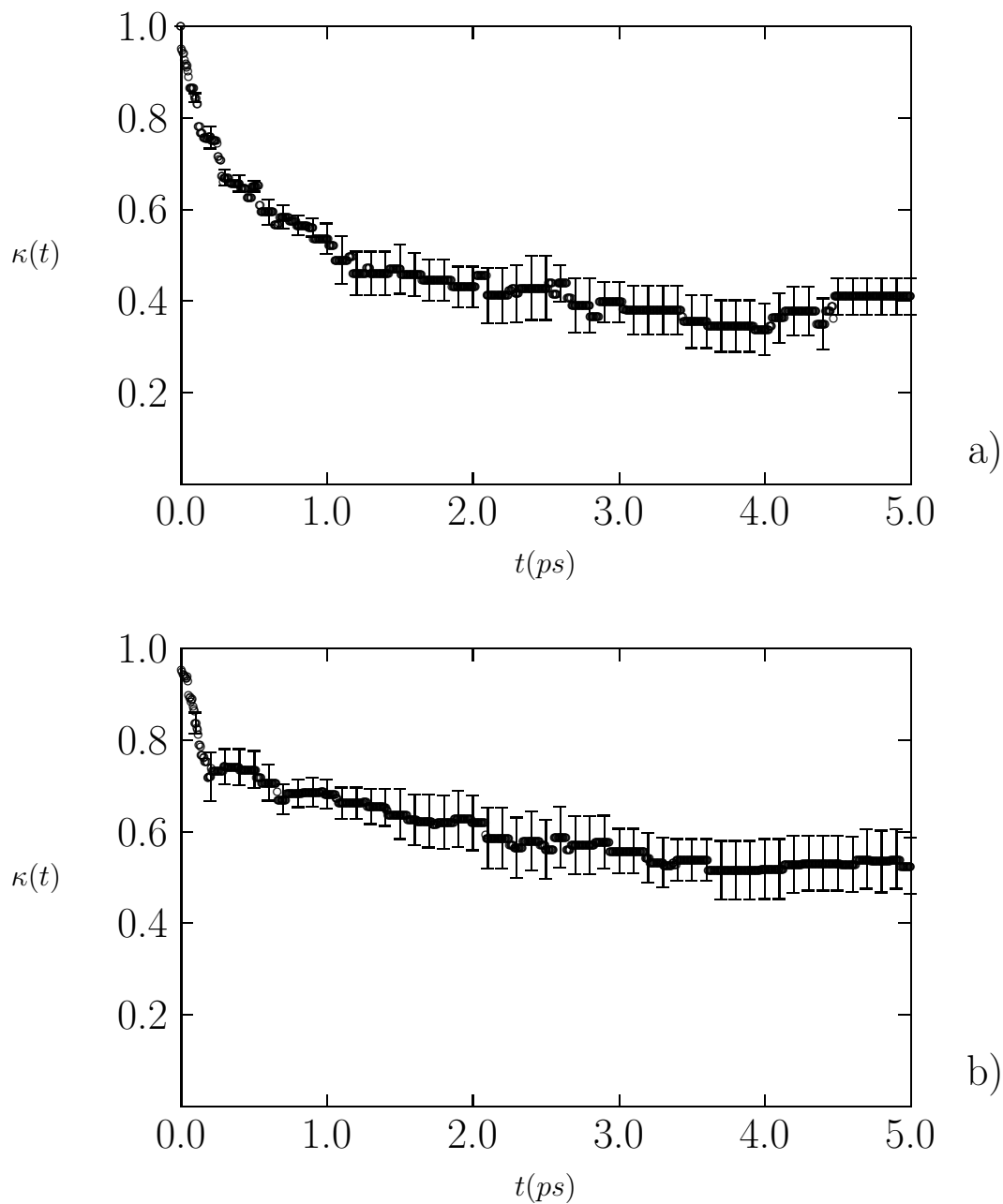


FIG. 13. Transmission coefficient as a function of time for (a) a 67-solvent molecule cluster and (b) a 20-solvent molecule cluster.